Mechanics of Materials 142 (2020) 103275

Contents lists available at ScienceDirect

Mechanics of Materials

journal homepage: www.elsevier.com/locate/mechmat

Research paper

Design of nano-modified PVDF matrices for lead-free piezocomposites: Graphene vs carbon nanotube nano-additions

Jagdish A. Krishnaswamy[a,*], Federico C. Buroni[b], Enrique García-Macías[c], Roderick Melnik[a,d], Luis Rodriguez-Tembleque[d], Andres Saez[d]

[a] MS2Discovery Interdisciplinary Research Institute, Wilfrid Laurier University,75 University Ave W, Waterloo, Ontario, Canada N2L 3C5
[b] Department of Mechanical Engineering and Manufacturing, Universidad de Sevilla,Camino de los Descubrimientos s/n, Seville E-41092, Spain
[c] Department of Civil and Environmental Engineering, University of Perugia,Via G Duranti 93, Perugia 06125, Italy
[d] Department of Continuum Mechanics and Structural Analysis, Universidad de Sevilla,Camino de los Descubrimientos s/n, Seville E-41092, Spain

ARTICLE INFO

Keywords:
lead-free piezocomposites
micromechanics
finite element analysis
PVDF
homogenization
coupled models
graphene
carbon nanotubes

ABSTRACT

Graphene nano-additions to polymer matrices have demonstrated exceedingly better mechanical properties compared to carbon-nanotube modified matrices. Therefore, in the context of mechanically superior high-performance piezo-composites, graphene-modified composite architectures represent an important design direction. In this paper, we first develop an effective property model for graphene-modified piezoelectric matrices, taking into account the mechanical anisotropy of the matrix. We further evaluate the piezoelectric performance of the matrix architecture which incorporates lead-free $BaTiO_3$ polycrystal inclusions. In order to obtain comparisons with well-established composites, we compare the electro-elastic response of two composite architectures in which the matrix is modified by multiwalled CNTs and graphene respectively. It is seen that, near percolation of the nano-additions, graphene-based systems exhibit an order of improvement in the piezoelectric response compared to the composite without nano modification. This improvement is comparable to CNT-based systems, but the matrix hardening is lesser than half the hardening observed in CNT-modified composites. This feature is due to a considerably smaller percolation threshold of graphene compared to CNTs which brings about percolative conditions at very small filler concentrations. We further investigate the dependence of the electric flux and fields in the graphene-modified piezocomposite on the polycrystallinity of the piezoelectric inclusions to identify the polycrystalline configurations that can lead to improved performance in such nanomodified piezocomposites.

1. Introduction

Carbon nanotubes and graphene are important nanomaterials in the area of functionalized smart composites. This is because both the materials simultaneously exhibit excellent mechanical (Shen and Li, 2005; Ovid'Ko, 2013) and electronic properties (Dürkop et al., 2004; Bolotin et al., 2008), with extremely high Young's moduli (in the TPa range) as well as extremely high charge carrier mobilities (exceeding several thousands of cm^2/Vs). Their ability to impart these properties to a matrix material has generated interest in the design of nanocomposites with excellent electro-mechanical properties. Although carbon nanotubes are well-understood and established as nanofillers for enhancing the elastic and electrical properties of nanocomposites, graphene-based composites have been shown to exhibit exceedingly better mechanical behavior (Rafiee et al., 2009a; Rafiee et al., 2009b; Rafiee et al., 2010) in terms of improved Young's moduli, improved fracture strength, reduced crack propagation and improved buckling resistance. These improvements mainly stem from the relatively larger interfacial area between graphene and the matrix and consequent better adhesion between the two components. Further, graphene also improves the electrical conductivity of the matrix through the formation of percolative conductive networks of highly conductive graphene fragments (Kim et al., 2010). Therefore, graphene modified polymer matrices are an important starting point in the design of functional nanocomposites which can exhibit significantly superior mechanical and electrical behaviors.

In this paper, we compare the design of two nano-modified lead-free piezocomposites based on piezoelectric polyvinylidene difluoride (PVDF) matrices. The designs include the modification of the PVDF matrix through addition of either multiwalled carbon nanotubes

* Corresponding author.
E-mail address: ajagdish@wlu.ca (J.A. Krishnaswamy).

https://doi.org/10.1016/j.mechmat.2019.103275
Received 10 September 2019; Received in revised form 8 December 2019; Accepted 8 December 2019
Available online 16 December 2019
0167-6636/ © 2019 Elsevier Ltd. All rights reserved.

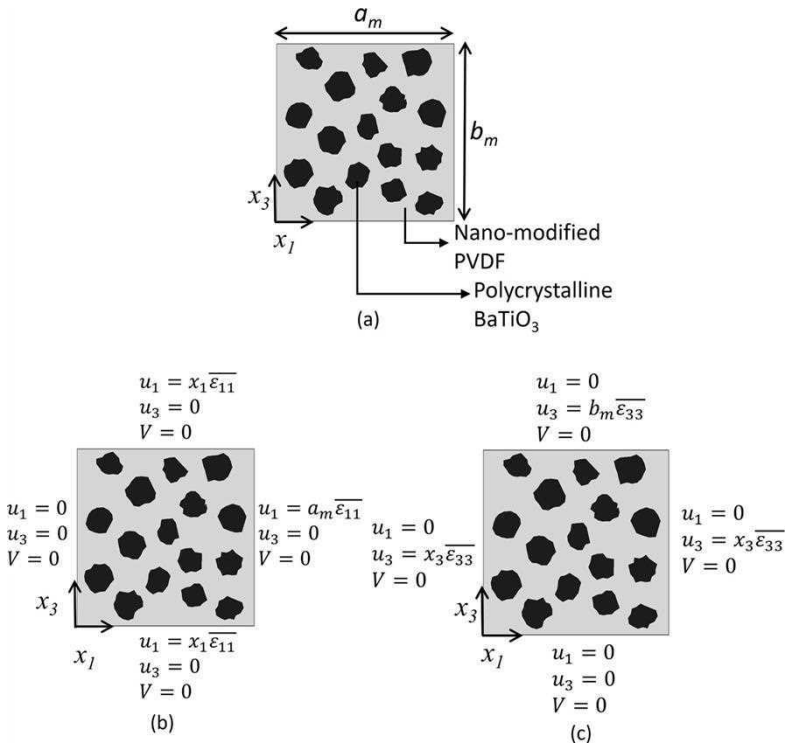

Fig. 1. (a) Schematic of the RVE investigated in this analysis with the coordinate system and RVE dimensions, (b) and (c) boundary conditions BC1 and BC2, respectively, used to obtain the effective piezoelectric coefficients e_{31} and e_{33} respectively.

(MWCNTs) or graphene. Piezocomposites are materials which bring together favorable mechanical properties of a host matrix material and the piezoelectric properties of inclusions. Fibrous composites and their homogenization have been a well-studied topic in the modeling of the effective properties of these materials (Dai and Ng, 2012; Kuo and Bhattacharya, 2013). Here we will look at the effect of randomly shaped piezoelectric inclusions within a piezoelectric PVDF matrix with anisotropic elastic properties.

We bring together our theoretical understanding of the effective elastic properties of carbon nanotube- (CNT-) and graphene-modified PVDF matrices and lead-free piezocomposite design using microscale polycrystalline $BaTiO_3$ inclusions. We first develop a model for the effective elastic properties of graphene-modified PVDF. This model takes into account the elastic anisotropy of PVDF. We further use these effective elastic coefficients in the design of lead-free piezocomposites with polycrystalline $BaTiO_3$ embedded in the nano-modified PVDF matrix. Further, we compare this composite design with the well-established CNT-modified piezocomposite design. Such a comparison leads to a better understanding of design contexts where using graphene as a nanofiller might be beneficial compared to CNTs. We observe major differences in the performance of these two variants of composite design because of the considerable differences in the elastic properties and dielectric (percolation parameters). The main aspects of comparison include the effective piezoelectric flux response, the electric field response, and the optimal polycrystallinity of inclusions leading to optimal electric flux generation.

2. Electro-elastic model and material property models

In this section, we provide details of the coupled electro-elastic model describing the piezoelectric response of the composites followed by the details of the material properties and models used in the simulations. The analysis combines the development of models for effective properties of nanomaterial-modified matrices and coupled electro-elastic models which incorporate the effective homogenized matrix properties to evaluate the piezo-response using representative volume elements (RVE), which is a well-understood route to predict nanomodified piezocomposite behavior (Hasanzadeh et al., 2019).

The composite architecture is modeled as a representative volume element in two-dimensions ($x_1 - x_3$ plane). The geometry of the composite consists of randomly shaped lead-free microscale $BaTiO_3$ inclusions embedded in random positions within a square shaped matrix of sides $a_m = b_m = 50$ μm (Fig. 1(a)). The matrix is modified with a uniform distribution of two types of non-agglomerated nanomaterials – (15,15) multiwalled carbon nanotubes (MWCNTs) and graphene. The phenomenological and governing balance equations describing the electro-elastic behavior of the composites, respectively, are (Saputra et al., 2018; , Krishnaswamy et al., 2019b):

$$\sigma_{ij} = c_{ijkl}\varepsilon_{kl} - e_{kij}E_k, \quad D_i = \epsilon_{ij}E_j + e_{ijk}\varepsilon_{jk}, \tag{1}$$

$$\sigma_{ij,j} = 0, \quad D_{i,i} = 0, \tag{2}$$

where σ_{ij} and ε_{ij} are the stress and strain tensor components, respectively, and E_i and D_i are the components of the electric field and the electric flux density vectors, respectively. The material-dependent factors c_{ijkl}, e_{ijk}, ϵ_{ij} are the elastic, piezoelectric and the permittivity coefficients of the constituent materials of the composite. The relation between the strain and the displacement is given by $\varepsilon_{ij} = \frac{1}{2}(u_{i,j} + u_{j,i})$. The implementation of the model in two-dimensions and the algorithms used to generate random polygonal inclusions can be found in (Krishnaswamy et al., 2019b). The composite RVE is further subjected to two boundary conditions BC1 and BC2 as shown in Fig. 1(b)–(c), to

Table 1
Elastic coefficients of the PVDF matrix (Odegard, 2004), $BaTiO_3$ single crystal inclusions (Berlincourt and Jaffe, 1958), (15,15) MWCNTs (Shen and Li, 2005), and graphene (Ji et al., 2010; Garcia-Macias et al., 2018).

Elastic coefficients (in GPa)	Values for PVDF (Odegard, 2004)	Values for $BaTiO_3$ (single crystal (Berlincourt and Jaffe, 1958))	Values for (15,15) MWCNT (Shen and Li, 2005)	Values for graphene (Ji et al., 2010; Garcia-Macias et al., 2018)
c_{11}	3.8	275.1	230.1	1219
c_{12}	1.9	178.9	211.9	481
c_{13}	1.0	151.55	66.3	6.8
c_{22}	3.2	275.1	230.1	1219
c_{23}	0.9	151.55	66.3	6.8
c_{33}	1.2	164.8	1429.9	102,000
c_{44}	0.7	54.3	398	102,000
c_{55}	0.9	54.3	398	102,000
c_{66}	0.9	113.1	9.1	369

obtain the effective piezoelectric coefficients e_{31} and e_{33}, respectively (Qin et al., 2014; Sladek et al., 2016; Saputra et al., 2018; Krishnaswamy et al., 2019b). The principle of homogenization is to evaluate the volume averages of the electro-elastic parameters of interest and subsequently to compute the effective electro-elastic coefficients of the RVE. In the present case, the boundary conditions BC1 and BC2 impose the volume averages described by Eqs. (3a) and (3b), respectively:

$$\varepsilon_{11} = \overline{\varepsilon_{11}}, \quad \varepsilon_{33} = 0, \quad \varepsilon_{13} = 0, \quad E_1 = E_3 = 0, \tag{3a}$$

$$\varepsilon_{11} = 0, \quad \varepsilon_{33} = \overline{\varepsilon_{33}}, \quad \varepsilon_{13} = 0, \quad E_1 = E_3 = 0. \tag{3b}$$

Following this, the effective electroelastic coefficients of interest, e_{31}^{eff} and e_{33}^{eff} are evaluated using BC1 and BC2, respectively, as

$$e_{31}^{eff} = \frac{1}{A}\frac{D_3}{\overline{\varepsilon_{11}}}, \tag{4a}$$

$$e_{33}^{eff} = \frac{1}{A}\frac{D_3}{\overline{\varepsilon_{33}}}, \tag{4b}$$

where A is the area of the two-dimensional RVE (volume in three dimensions), given by $A = a_m b_m$. In Eqs. (3) and (4), * indicates the volume average of the quantity *. The coefficients evaluated using Eqs. (4a) and 4b) represent the transverse and longitudinal piezoelectric response of the composite in two dimensions. The development and use of such specialized boundary conditions for evaluating effective material properties through homogenization can be found in (Sladek et al., 2016; Saputra et al., 2018; Benedetti et al., 2019). Specifically, the effective properties evaluated using these boundary conditions allow designing macroscopic composite structures obtained by spatially repeating the RVE which possesses the effective properties evaluated by the approaches highlighted in Eqs. (3) and ((4). The details of the RVE geometry investigated here are given in the Appendix A1. The inclusions are geometrically modelled as a polygon with a random number of edges, n, chosen in the interval [10–20]. Further, the random vertices of the polygon are bounded within two concentric circles with random radii R1 and R2, which are selected in the ranges [2.5 μm, 3.5 μm] and [4 μm, 5 μm], respectively. We further assume that the inclusions are not in contact with each other. Inclusions having contact can lead to locally efficient electrical and mechanical coupling and therefore can lead to better performance. However, we consider the worst-case scenario where such enhancements do not exist, and hence maintain noncontact conditions between the inclusions. Further, the geometry is simplified in such a way that the inclusions do not have contact with the boundaries of the RVE. We expect that this assumption will not affect noticeably the evaluation of the effective properties. Appendix A1, further, also provides the information relating to the effect of the RVE size on the estimated effective properties.

Table 2
The dielectric and piezoelectric properties of the matrix (PVDF) and inclusions ($BaTiO_3$).

Material property	Values for $BaTiO_3$	Values for PVDF
Relative permittivity		
ϵ_{11}/ϵ_0	1970 (Berlincourt and Jaffe, 1958)	8 (Odegard, 2004)
ϵ_{33}/ϵ_0	109	8
Piezoelectric coefficients (Cm^{-2})		
e_{15}	21.3 (Berlincourt and Jaffe, 1958)	0 (Odegard, 2004)
e_{31}	−2.69	0.024
e_{33}	3.65	−0.027

We next briefly discuss the material properties used in this investigation. The PVDF matrix and the $BaTiO_3$ inclusions are anisotropic in their electro-elastic behavior. Further, the $BaTiO_3$ inclusions are assumed to be polycrystalline, the anisotropic properties of which are derived from the single crystal data as detailed in (Li, 2000; Krishnaswamy et al., 2019b). Further, the matrix is modified by two types of nanofillers – (15,15) MWCNTs and graphene and the effective elastic properties of the matrix are obtained using the elastic properties of the nanofiller. The elastic coefficients of the PVDF matrix, $BaTiO_3$ single crystals, (15,15) MWCNTs, and graphene are presented in Table 1. Table 2 further lists the dielectric and piezoelectric properties of the PVDF matrix and single crystal $BaTiO_3$.

The effective elastic properties of the nano-modified PVDF matrices are obtained by using a classical Mori-Tanaka model which takes into account the anisotropic elastic coefficients of the matrix and the nanofiller, summarized in Table 1. Details of this methodology can be found in (Krishnaswamy et al., 2019a).

Nanofillers further modify the dielectric properties of the matrix (Gaiser et al., 2015). The effective permittivity of the modified matrix has a percolative dependence on the nanofiller concentration given by (Pecharroman et al., 2001):

$$\epsilon_m^{eff} = \epsilon_m \left(\frac{f_c}{f_c - f_{\text{nano}}} \right)^p, \tag{3}$$

where ϵ_m and ϵ_m^{eff} are the permittivity of the pristine and the nano-modified matrices respectively, f_c and p are the percolation threshold and critical exponent which depend on both the nanofiller and the matrix, and f_{nano} is the concentration of the nanofiller in the matrix. Eq. (3) implies a rapid increase in the effective permittivity of the modified matrix as the filler concentration f_{nano} approaches the percolation threshold f_c and the increase is more pronounced for higher values of the critical exponent p. We obtain the percolation parameters from experimental measurements on PVDF matrices with uniformly dispersed nanofillers. In the case of MWCNTs with an approximate aspect ratio of 100, $f_c = 1.14\%$ and $p = =1.0068$ (Yao et al., 2007). In the case of graphene, the percolation threshold is much smaller, with $f_c = 0.18\%$ and $p = =1.09$ (Fan et al., 2012). We emphasize here that adding more nanofiller to a matrix beyond the percolation threshold

will lead to electrical shorting of the material and render it unusable and thus the percolation threshold is considered as the upper limit of nano-additions here. The piezoelectric response of the matrix is related to its β-phase content, which is influenced by the addition of nanofillers (Lee et al., 2008; Kim et al., 2009; Huang et al., 2014). We note that this dependence is not completely characterized and the available data suggests a weak dependence which can be ignored considering much larger piezoelectric coefficients of the $BaTiO_3$ inclusions, and hence we model the piezoelectric coefficients of the matrix as constants given by the values of the pristine matrix. The polycrystallinity of the $BaTiO_3$ inclusions is an important design parameter. The effective electro-elastic properties of polycrystalline inclusions, the material model used to derive these quantities and the relevance of polycrystalline inclusions in piezocomposite design have been discussed elsewhere (Li, 2000; Krishnaswamy et al., 2019b). The effective electro-elastic coefficients of polycrystalline inclusions are derived starting from the coefficients of $BaTiO_3$ single crystals (Li, 2000). The extent of polycrystallinity is quantified by using parameter α, such that $\alpha \to 0$ and $\alpha \to \infty$, respectively, correspond to the single crystalline and randomly oriented conditions. Values of α in between these extreme limits correspond to a controlled randomness with net orientation of grains along the poling direction (x_3 direction). The value of α depends on several factors including the crystal quality, poling conditions and so on (Li, 2000). The composite is assumed to be poled along the x_3 direction. However, within the polycrystalline inclusions, the poling axes (or the c-axes) of the individual domains are oriented in different directions, following a transversely isotropic distribution of orientation angles θ with respect to the x_3 direction. These orientation angles (or polarization angles) must be accounted for to obtain a homogenized effective model for polycrystalline piezoelectric aggregates (Benedetti et al., 2019). We assume, as indicated in (Li, 2000), that the orientation distribution follows a Gaussian distribution given by

$$W = \frac{1}{\alpha\sqrt{2\pi}} e^{-\frac{\theta^2}{2\alpha^2}}. \tag{4}$$

We therefore see that α is the standard deviation of the orientation distribution function W.

3. Results and discussion

Although graphene leads to a significantly higher hardening of the matrix compared to a matrix modified by the same volume fraction of non-agglomerated nanotubes (see details in Appendix A2), the graphene-based architecture has a much lesser percolation threshold. The implication of this is that adding more graphene to a percolated composite matrix will lead to electrical shorting and hence it is not possible in the context of a piezoelectric device. Therefore, when it comes to the maximum matrix hardening possible with a given nanomaterial, we are limited by the percolation threshold of the nanomaterial. Hence, we see that at percolation, the nanotube-modified matrices have around a 100% increase in the elastic coefficients, implying significant hardening. However, in the case of graphene, the increase is not so significant and is around a maximum of 50%. However, the permittivities of both matrices follow a percolative dependence on the volume fraction of the nanomaterial in the matrix.

This means that near percolation conditions, the graphene-modified matrix is significantly softer than the CNT-modified matrix, while having similar significant improvements in the effective matrix permittivity. This is an advantage in the context of individually tailoring the mechanical and electrical properties of the composite. It is possible to significantly boost the permittivity while retaining the softness of the host matrix. In this particular case, it will be a considerable advantage, for example, in the design of wearable or flexible devices which can sense or harvest energy from mechanical stimuli. These devices require soft composites exhibiting appreciable electrical performance for which design strategies that allow boosting the electrical performance while not hardening the matrix further, are desired. It is also clear from Fig. 2(d)–(e) that both the CNT- and graphene- modified matrices lead to a percolative improvement in the piezoelectric response with a significant improvement near percolation (shown for a polycrystallinity index of $\alpha = 0.3$, which is near the optimal value for best piezoelectric response). Based on this observation, all the analyses that follow are based on the behavior of the composite near percolation conditions, which is modeled as $f_{CNT} = 0.99 f_c$.

Fig. 3(a)–(c) and (d)–(f), respectively, show the effective piezoelectric coefficients e_{31} and e_{33} of the two composite architectures

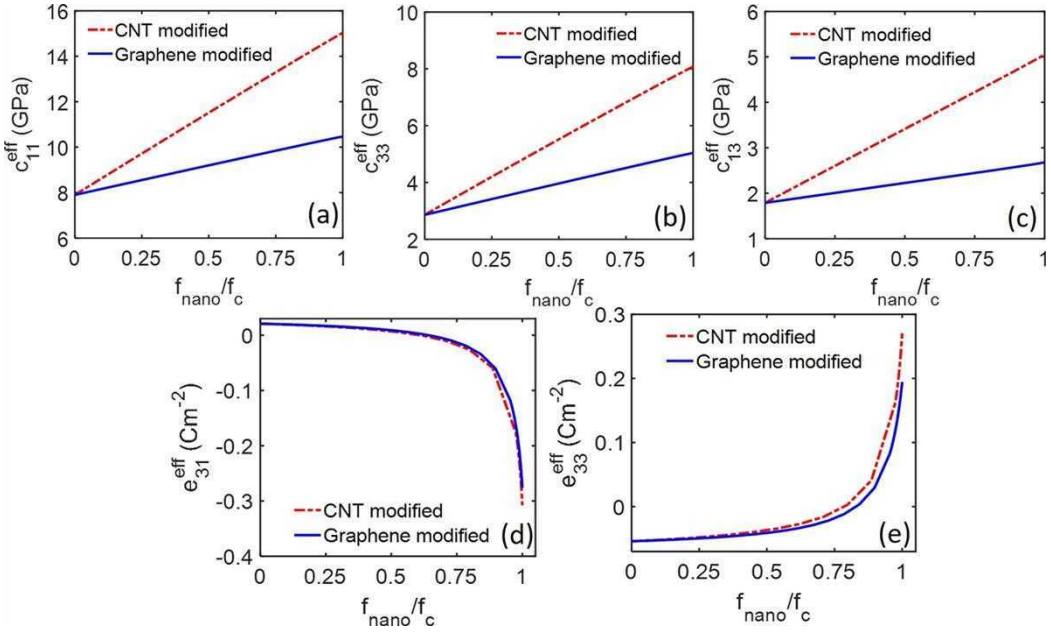

Fig. 2. Plots (a)–(c) in sequence show the effective elastic coefficients c_{11}, c_{33}, and c_{13} of both nano-modified PVDF matrices as a function of the nanofiller concentration f_{nano} normalized by the percolation threshold f_c of the corresponding nanofiller. Plots (d) and (e) show a percolative dependence of the effective piezoelectric coefficients e_{31} and e_{33} of the composite as a function of the normalized nanofiller concentration.

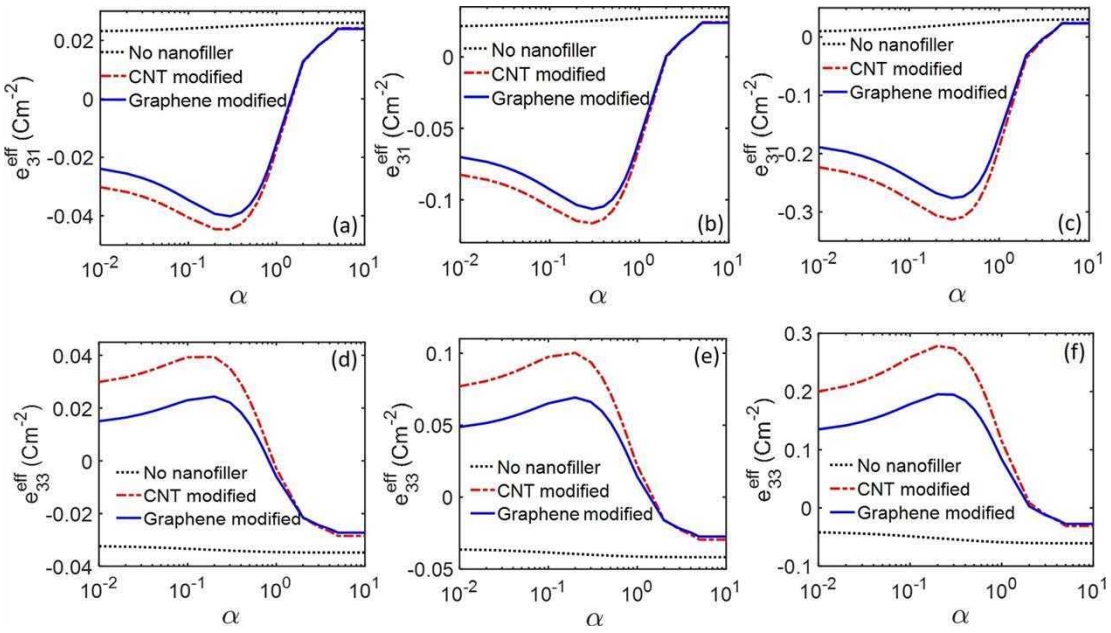

Fig. 3. Effective transverse and longitudinal piezoelectric coefficients, e_{31} and e_{33} respectively, of the nano-modified PVDF/$BaTiO_3$ composites, as a function of the polycrystallinity index α, for different $BaTiO_3$ inclusion concentrations V_{BTO} : Plots (a) and (d) correspond to V_{BTO} = 14.7%, plots (b) and (e) correspond to V_{BTO} = 25.9%, and plots (c) and (f) correspond to V_{BTO} = 41.2%.

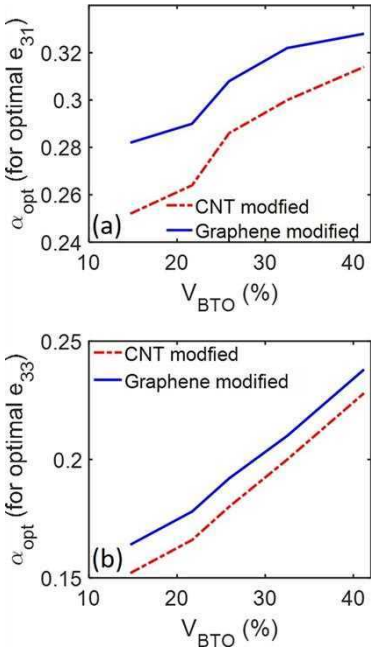

Fig. 4. Optimal polycrystallinity index α_{opt} leading to the highest piezoelectric flux response of the composite under percolative nanofiller loading (f_{nano} = $0.99f_c$). Plot (a) corresponds to e_{31} and plot (b) corresponds to e_{33}.

which are modified by CNTs and graphene. The results corresponding to very dilute $BaTiO_3$ loading are not presented here. This is because $BaTiO_3$ and PVDF have piezoelectric tensor coefficients (specifically, e_{31} and e_{33}) which are of opposite signs, owing to which, the addition of $BaTiO_3$ negates the piezoelectric activity of the PVDF and reduces the overall response of the composite for low $BaTiO_3$ concentrations. We have discussed this aspect earlier (Krishnaswamy et al., 2019a). However, once the $BaTiO_3$ concentration exceeds a certain limit, the effective piezoelectric response of the matrix, especially in the presence of a percolated nano-modified matrix, is predominantly controlled by the $BaTiO_3$ inclusions with the matrix piezoelectricity contributing negligibly (Krishnaswamy et al., 2019a). Accordingly, we see that in the case of both the nano-fillers, there is a significant increase in the piezoelectric response coefficients e_{31} and e_{33}. At higher inclusion concentrations, Fig. 3(c) and (f) indicate that an improvement of more than an order of magnitude is possible through graphene or CNT addition to the matrix. However, the piezoelectric response of graphene-based composites is still smaller compared to the CNT-based composites. This is mainly because of reduced matrix-hardening. Although graphene-based designs do not exceed the performance of CNT-based designs, an order of magnitude improvement in the piezoelectric response is still possible, compared to composites which are not nano-modified, while appreciably retaining the mechanical properties of the matrix. This observation is also in agreement with recent experimental work on graphene-modified PVDF/$BaTiO_3$ piezocomposites (Shi et al., 2018).

From Fig. 3(a)–(f), it is also seen that the polycrystalline index α, at which optimum piezoelectric response results, is slightly different for CNTs and graphene. This could be due to a combination of the following factors – the difference in the elastic properties of the matrix at percolation and the difference in the permittivity of the matrix at percolation – which vary across the designs. Notably, although the graphene-modified PVDF matrix has much smaller elastic moduli compared to the CNT-modified matrices, the permittivity of the graphene-based system is relatively higher at percolation. From Eq. (3), we understand that when f_{CNT} = $0.99f_c$, the enhancement in the permittivity in graphene-modified PVDF is around 150 times of the pristine PVDF permittivity, while in the case of CNT-modified PVDF, the enhancement is around 100.

In Fig. 4(a)–(b), we further plot the optimal α which leads to maximum piezoelectric flux generation (i.e. maximum e_{ij}) for both piezocomposite architectures (CNT-modified and graphene-modified), as a function of the volume fraction of the $BaTiO_3$ inclusions, V_{BTO}. First, we notice that the optimal polycrystalline index for graphene-modified systems is slightly higher consistently, for all V_{BTO}, compared to the CNT-modified system. Further, the optimal polycrystalline index increases with an increase in V_{BTO}. These results have the following implications: (a) graphene-nanomodifications can allow the use of slightly more polycrystalline piezoelectric inclusions for optimum performance and therefore allow more tolerances in the processing of high

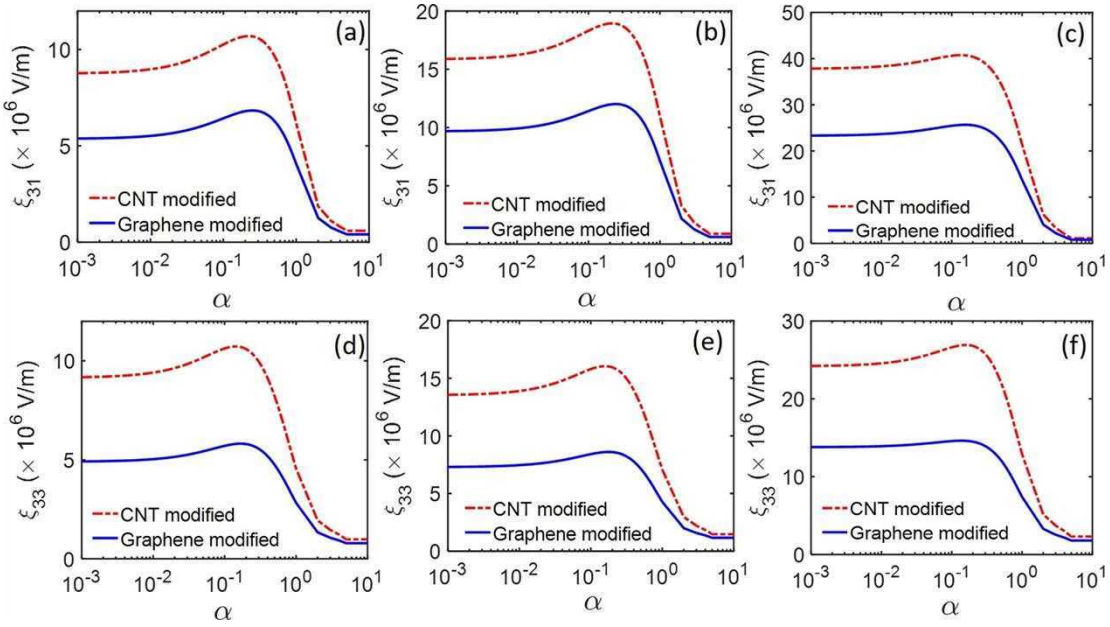

Fig. 5. Volume averaged electric field normalized by the applied strain, as a function of the polycrystallinity index α, for different $BaTiO_3$ inclusion concentrations V_{BTO}. Plots (a)–(c) correspond to the transverse response ξ_{31} and plots (d)–(f) correspond to the longitudinal response ξ_{33}. As in Fig. 3, plot pairs (a) and (d), (b) and (e), and (c) and (f) correspond to V_{BTO} = 14.7%, 25.9%, and 41.2%, respectively.

quality piezoelectric crystals, and (b) higher $BaTiO_3$ inclusion concentrations allow the introduction of higher polycrystallinity to maximize the piezoelectric response.

We further point out that the effectiveness of a piezocomposite material is measured by its ability to simultaneously generate high electric flux and electric fields (Priya, 2010; Maurya et al., 2018). In fact, the product of the piezoelectric flux coefficient and the field coefficient ($d_{ij}g_{ij}$) is a measure of the energy density in a piezocomposite. Usually, there is a tradeoff between the flux and field generating processes (Maurya et al., 2018) and effective design needs to take into consideration a balance between these processes. In this context, we explore the electric field coefficient in the CNT- and graphene-modified composites, given by:

$$\xi_{ij} = \frac{E_i}{\overline{\varepsilon_j}}, \tag{5}$$

where the numerator in the right-hand side is the RVE-volume-averaged electric field, and the denominator is the applied boundary strain (refer to Fig. 1(b) and (c)) in the Voigt notation. For example, ξ_{31} is the ratio of the volume averaged electric field generated in the x_3 direction normalized by the axial strain in the x_1 direction (i.e. $\overline{\varepsilon_{11}} = \overline{\varepsilon_1}$). Given the present two-dimensional context, we will refer to ξ_{31} and ξ_{33} as the transverse and longitudinal electric field coefficients, respectively.

We present the transverse and longitudinal electric field coefficients, ξ_{31} (Fig. 5(a)–(c)) and ξ_{33} (Fig. 5(d)–(f)), respectively, for three different volume fractions. We note that the electric field generated in the graphene-based composite is smaller than in the case of the CNT-based composite, irrespective of the polycrystallinity index α. This is because of the higher permittivity of the graphene-modified PVDF matrix near percolation, as pointed out earlier, compared to the CNT-modified matrix. This increased permittivity is due to the differences in the percolation properties of CNTs and graphene, where particularly graphene has a slightly larger critical exponent which gives larger permittivity enhancements due to the percolative effect. It is thus evident that an optimal critical exponent p is necessary to obtain a permittivity which is high enough to obtain a large permittivity to support the flow of electric flux from the high-permittivity inclusion environment through the surrounding matrix. However, it should be low enough to ensure that the electric fields within the composite do not get compromised. The critical exponent, as seen from experimental literature on CNT-based composites (Li et al., 2008), is tunable through chemical functionalization of the nanotubes.

One can envisage such an atomic/molecular level design even for graphene-based composites to further tune the critical exponent to an optimal value. Also, the dependence of the electric field response on the polycrystallinity and the existence of an optimal α for maximum electric field generation gradually fades out at higher inclusion concentrations, unlike in the case of the electric flux response where clear local maxima exist even at higher inclusion concentrations.

In summary, we have observed that significant enhancements (an order of magnitude) in the electric flux generation are possible in both CNT and graphene-modified PVDF matrices. However, in contrast to CNT-modified composites, the considerably smaller percolation threshold in the case of graphene can allow such improvements in flux generation without significant matrix hardening. Secondly, the higher permittivity of graphene-modified composite at percolation results in reduced electric field generation compared to CNT-modified composites. Thirdly, we have noticed that the optimal inclusion polycrystallinity leading to maximum flux generation, at percolation, is slightly higher in the case of the graphene-based composite and this optimal value increases with increasing inclusion concentration indicating that polycrystal-based designs could be more useful in composites with larger inclusion concentrations. From the perspective of design, this means that a larger quantity of inexpensive of microscale polycrystals can lead to a better design compared to high-quality single-crystal inclusions.

4. Conclusions

We have explored the design of nano-modified PVDF-based lead-free piezocomposites by developing a new effective property model accounting for the elastic anisotropy in PVDF. Using this modeling approach, we have compared the performance of piezocomposites modified by carbon-nanotubes and graphene. While CNT addition is a well understood route to boost piezoelectric response, graphene holds more promise in terms of better mechanical properties of the modified

matrix. Firstly, in terms of piezoelectric response, although the graphene-based design results in lesser electric flux generation compared to the CNT-based design, it can still lead to an order of magnitude improvement near percolative conditions compared to composites which are not nano-modified. Secondly, with increasing inclusion concentrations, the optimal inclusion-polycrystallinity for maximum flux generation also increases, thus pointing to the fact that using larger quantities of polycrystalline materials could lead to optimum performance and practically viable solutions to superior piezoelectric performance. Thirdly, graphene-based designs generate smaller electric fields compared to CNT-based designs because of higher matrix permittivity at percolation. Lastly, the graphene-modified composites require piezoelectric inclusions of slightly higher polycrystallinity, compared to CNT-modified composites, for optimum flux generation. This indicates that using graphene as a nano-modifier allows for slightly more process intolerances in the processing of high quality of piezo-crystals, which would directly impact the cost of their production. Also, in both the composite systems, the optimum polycrystallinity for best flux generation at percolation of the nanofiller, increases as the piezoelectric inclusion concentration is increased. This further suggests that using larger quantities of relatively more polycrystalline piezo-crystals might be an interesting route to maximize piezo-response in a scalable manner. In conclusion, we note that graphene-modified piezo-composites provide improvements similar to CNT-modified systems, while allowing for higher inclusion polycrystallinity and better retention of the matrix elasticity. This makes graphene a viable alternative to CNTs especially in application requiring flexible high-performance piezocomposites.

Author role

JAK did the finite element calculations and prepared the initial draft of the manuscript. EGM and LRT did the calculations of effective elastic properties, based on the two-parametric model, while FCB provided inputs on the theoretical aspects of such models. AS and RM designed research and contributed to all its aspects. All authors reviewed the manuscript and gave approval to its final version.

Declaration of Competing Interest

None.

Acknowledgments

This work was supported by the Ministerio de Economía y Competitividad of Spain and the European Regional Development Fund under projects RTI2018-094945-B-C21 and DPI2017-89162-R. The financial support is gratefully acknowledged. RM and AKJ are also grateful to the NSERC and CRC program for their support.

Appendices

A1. Details of the RVE geometries

The RVEs investigated here with the inclusion volume fraction V_{BTO} of the $BaTiO_3$ inclusions are shown in Fig. AF1(a)–(e).

The effect of the RVE size has been analyzed for similar architectures in our earlier studies (Krishnaswamy et al., 2019). The plots in Fig. AF2 provide an example of the study conducted on a PDMS(matrix)/$BaTiO_3$(inclusion) composite with randomly shaped and positioned inclusions. We see that for all the inclusion volume fractions (V_{BTO}) considered the standard deviation in the evaluated effective coefficient e_{31} (Fig. AF2(b)) is at

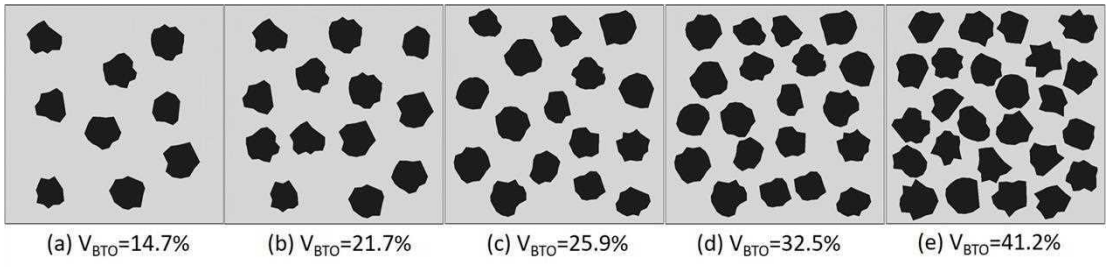

Fig. AF1. The RVEs investigated in this analysis with different inclusion volume fractions, V_{BTO}.

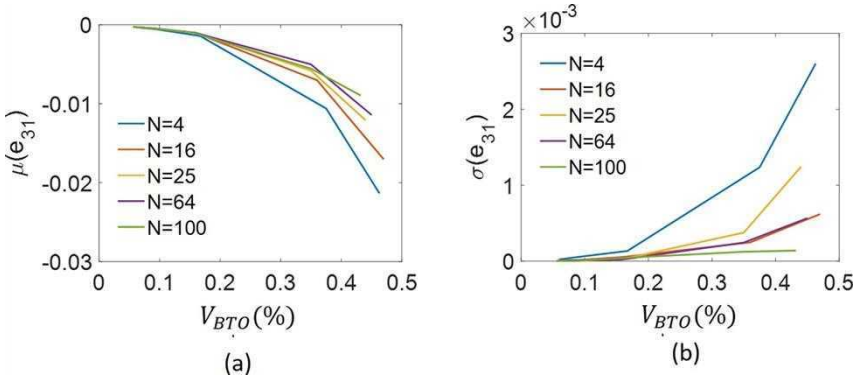

Fig. AF2. Numerical results to evaluate the effect of the RVE size for different inclusion concentrations V_{BTO}. Here N represents the number of inclusions in the RVE. Plots (a) and (b) show the mean and the standard deviation, respectively, of the effective coefficient e_{31} of the composite.

least an order of magnitude lesser than the mean value (Fig. AF2(a)). As expected, the standard deviation reduces as the number of inclusions N increases for a given inclusion concentration. In our analysis, we adopt an RVE size that is intermediate to the extremely large and the extremely small limits considered in this study. For example, in our study, an inclusion concentration of $V_{BTO} = 41.2\%$ is represented by an RVE with $N = 25$ inclusions. For this study, the averaging was carried out over 5 RVE architectures for each data point (i.e. for each combination of V_{BTO} and N).

A2. Effective elastic coefficients of nano-modified PVDF

Fig. AF3 shows the effective elastic coefficients, relevant to the two-dimensional analysis carried out here. Graphene has a significantly larger (> 50%) hardening effect compared to CNTs. However, at percolation, due to much smaller percolation thresholds in the case of graphene, the matrix hardening is considerably lesser than the CNT-modified PVDF, as would be seen from Fig. 2.

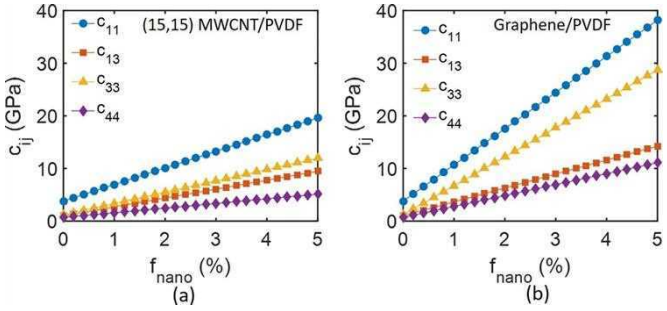

Fig. AF3. Effective elastic coefficients of (a) *k*CNT-modified PVDF and (b) Graphene-modified PVDF, as a function of the nanofiller concentration f_{nano}.

References

Benedetti, I., Gulizzi, V., Milazzo, A., 2019. A microstructural model for homogenisation and cracking of piezoelectric polycrystals. Comput. Methods Appl. Mech. Eng. 357, 112595.

Berlincourt, D., Jaffe, H., 1958. Elastic and piezoelectric coefficients of single-crystal barium titanate. Phys. Rev. 111 (1), 143.

Bolotin, K.I., Sikes, K.J., Jiang, Z., Klima, M., Fudenberg, G., Hone, J., Kim, P., Stormer, H.L., 2008. Ultrahigh electron mobility in suspended graphene. Solid State Commun. 146 (9), 351–355.

Dai, Q., Ng, K., 2012. Investigation of electromechanical properties of piezoelectric structural fiber composites with micromechanics analysis and finite element modeling. Mech. Mater. 53, 29–46.

Dürkop, T., Getty, S., Cobas, E., Fuhrer, M., 2004. Extraordinary mobility in semiconducting carbon nanotubes. Nano Lett. 4 (1), 35–39.

Fan, P., Wang, L., Yang, J., Chen, F., Zhong, M., 2012. Graphene/poly (vinylidene fluoride) composites with high dielectric constant and low percolation threshold. Nanotechnology 23 (36), 365702.

Gaiser, P., Binz, J., Gompf, B., Berrier, A., Dressel, M., 2015. Tuning the dielectric properties of metallic-nanoparticle/elastomer composites by strain. Nanoscale 7 (10), 4566–4571.

Garcia-Macias, E., Rodriguez-Tembleque, L., Saez, A., 2018. Bending and free vibration analysis of functionally graded graphene vs. carbon nanotube reinforced composite plates. Compos. Struct. 186, 123–138.

Hasanzadeh, M., Ansari, R., Hassanzadeh-Aghdam, M.K., 2019. Evaluation of effective properties of piezoelectric hybrid composites containing carbon nanotubes. Mech. Mater. 129, 63–79.

Huang, L., Lu, C., Wang, F., Wang, L., 2014. Preparation of PVDF/graphene ferroelectric composite films by in situ reduction with hydrobromic acids and their properties. RSC Adv. 4 (85), 45220–45229.

Ji, X.-Y., Cao, Y.-P., Feng, X.-Q., 2010. Micromechanics prediction of the effective elastic moduli of graphene sheet-reinforced polymer nanocomposites. Model. Simul. Mater. Sci. Eng. 18 (4), 045005.

Kim, G.H., Hong, S.M., Seo, Y., 2009. Piezoelectric properties of poly (vinylidene fluoride) and carbon nanotube blends: β-phase development. PCCP 11 (44), 10506–10512.

Kim, H., Abdala, A.A., Macosko, C.W., 2010. Graphene/polymer nanocomposites. Macromolecules 43 (16), 6515–6530.

Krishnaswamy, J.A., Buroni, F.C., García-Macías, E., Melnik, R.V., Rodriguez-Tembleque, L., Saez, A., 2019a. Design of lead-free PVDF/CNT/BaTiO3 piezocomposites for sensing and energy harvesting: the role of polycrystallinity, nanoadditives, and anisotropy. Smart Mater. Struct.

Krishnaswamy, J.A., Buroni, F.C., Garcia-Sanchez, F., Melnik, R., Rodriguez-Tembleque, L., Saez, A., 2019b. Improving the performance of lead-free piezoelectric composites by using polycrystalline inclusions and tuning the dielectric matrix environment. Smart Mater. Struct. 28 (7), 075032.

Kuo, H.-Y., Bhattacharya, K., 2013. Fibrous composites of piezoelectric and piezomagnetic phases. Mech. Mater. 60, 159–170.

Lee, J.S., Kim, G.H., Kim, W.N., Oh, K.H., Kim, H.T., Hwang, S.S., Hong, S.M., 2008. Crystal structure and ferroelectric properties of poly (vinylidene fluoride)-carbon nano tube nanocomposite film. Mol. Cryst. Liq. Cryst. 491 (1), 247–254.

Li, J.Y., 2000. The effective electroelastic moduli of textured piezoelectric polycrystalline aggregates. J. Mech. Phys. Solids 48 (3), 529–552.

Li, Q., Xue, Q., Hao, L., Gao, X., Zheng, Q., 2008. Large dielectric constant of the chemically functionalized carbon nanotube/polymer composites. Compos. Sci. Technol. 68 (10–11), 2290–2296.

Maurya, D., Peddigari, M., Kang, M.-G., Geng, L.D., Sharpes, N., Annapureddy, V., Palneedi, H., Sriramdas, R., Yan, Y., Song, H.-C., 2018. Lead-free piezoelectric materials and composites for high power density energy harvesting. J. Mater. Res. 33 (16), 2235–2263.

Odegard, G.M., 2004. Constitutive modeling of piezoelectric polymer composites. Acta Mater. 52 (18), 5315–5330.

Ovid'Ko, I., 2013. Mechanical properties of graphene. Rev. Adv. Mater. Sci. 34 (1), 1–11.

Pecharroman, C., Esteban-Betegon, F., Bartolome, J.F., Lopez-Esteban, S., Moya, J.S., 2001. New percolative $BaTiO_3$–Ni composites with a high and frequency-independent dielectric constant (εr ≈ 80000). Adv. Mater. 13 (20), 1541–1544.

Priya, S., 2010. Criterion for material selection in design of bulk piezoelectric energy harvesters. IEEE Trans. Ultrason. Ferroelectr. Freq. Control. 57 (12), 2610–2612.

Qin, R.-S., Xiao, Y., Lan, H., 2014. Numerical simulation of effective properties of 3d piezoelectric composites. J. Eng. 2014.

Rafiee, M., Rafiee, J., Yu, Z.-Z., Koratkar, N., 2009a. Buckling resistant graphene nanocomposites. Appl. Phys. Lett. 95 (22), 223103.

Rafiee, M.A., Rafiee, J., Srivastava, I., Wang, Z., Song, H., Yu, Z.Z., Koratkar, N., 2010. Fracture and fatigue in graphene nanocomposites. Small 6 (2), 179–183.

Rafiee, M.A., Rafiee, J., Wang, Z., Song, H., Yu, Z.-Z., Koratkar, N., 2009b. Enhanced mechanical properties of nanocomposites at low graphene content. ACS Nano. 3 (12), 3884–3890.

Saputra, A.A., Sladek, V., Sladek, J., Song, C., 2018. Micromechanics determination of effective material coefficients of cement-based piezoelectric ceramic composites. J. Intell. Mater. Syst. Struct. 29 (5), 845–862.

Shen, L., Li, J., 2005. Transversely isotropic elastic properties of multiwalled carbon nanotubes. Phys. Rev. B 71 (3), 035412.

Shi, K., Sun, B., Huang, X., Jiang, P., 2018. Synergistic effect of graphene nanosheet and $BaTiO_3$ nanoparticles on performance enhancement of electrospun PVDF nanofiber mat for flexible piezoelectric nanogenerators. Nano Energy 52, 153–162.

Sladek, J., Sladek, V., Krahulec, S., Song, C., 2016. Micromechanics determination of effective properties of voided magnetoelectroelastic materials. Comput. Mater. Sci. 116, 103–112.

Yao, S.-H., Dang, Z.-M., Jiang, M.-J., Xu, H.-P., Bai, J., 2007. Influence of aspect ratio of carbon nanotube on percolation threshold in ferroelectric polymer nanocomposite. Appl. Phys. Lett. 91 (21), 212901.